Article

The Role of Water Hydrogen Bonds in the Formation of Associates and Condensates in Dispersions of Serum Albumin with Shungite Carbon and Quartz Nanoparticles

Sergey Rozhkov [1], Andrey Goryunov [1], Vladimir Kolodey [2], Lyubov Pron'kina [2] and Natalia Rozhkova [2,*]

[1]   Institute of Biology, Karelian Research CentreRAS, 185910 Petrozavodsk, Russia
[2]   Institute of Geology, Karelian Research Centre RAS, 186910 Petrozavodsk, Russia
*   Correspondence: rozhkova@krc.karelia.ru; Tel.: +7-911-4018702

Abstract: The role of the network of water hydrogen bonds in the regulation of the intermolecular interaction's responsible for colloidal stability of dispersions has been studied in order to search for general patterns of interaction between water, nanoparticles, and bio-macromolecules. Raman spectroscopy for mixed dispersions of bovine serum albumin (SA), shungite carbon nanoparticles (ShC NPs), and quartz nanoparticles (quartz NPs) was performed within the wave number range 3200–3600 cm^{-1}. The main spectral lines in this range are caused by the OH stretch vibrations of water molecules. We analyzed the state of the water hydrogen bonding network for dispersions of varied ratios of both fatty acid-containing and fatty acid-free SA macromolecules, ShC NPs, and silica NPs in the range 0.01–10 mg/mL. We used dynamic light scattering to control the sizes of the protein associates and protein associates with ShC NPs and quartz NPs. The strength of the hydrogen bonds in water depends essentially non-linearly, but in a qualitatively similar way, on the concentrations of the dispersion components. The initial strengthening of the bonds is followed by their loosening with a further increase in the concentration of the components. This is accompanied by the association of the dispersion components. We estimate the thickness of the protein corona layer as 20–25 nm for ShC NPs and 28–33 nm for quartz NPs, depending on the SA concentration. Colloidal stability of the aqueous dispersion is determined almost completely by an association of the protein with NPs. In contrast, colloidal stability of a pure protein solution is regulated by the formation of protein clusters of two main types and sizes. The association effects of SA with ShC NPs are evident in microscopic images of condensate films. The structures differ significantly for native and fatty acid-free SA in shape and size.

Keywords: albumin; fatty acid; shungite carbon nanoparticles; shungite quartz; Raman scattering; dynamic light scattering; hydrogen bonds; condensate films

1. Introduction

The last decades have been characterized by intensive studies of bio-physical and bio-chemical interactions of nanosized materials with bio-objects of different levels of complexity for their using in bio-nanomedicine and environmental risk assessment [1–6]. Proteins are the most important component of these interactions, largely due to the ability to form a protein corona [7,8]. This significantly affects the colloidal stability of the aqueous dispersions of nanoparticles (NPs) [9], their transport, and their optical properties [10]. Of all the variety of proteins, serum albumins (SAs) most often serve as model objects for the analysis of the biological activity of NPs. For example, they are used as sensors for conformational and phase changes during the interaction of bio-molecules with NPs of various natures during the formation of a protein corona [11]; for surface coatings [12], being the most widely used protein for surface passivation applications [13]; as bio-surfactants [14]; for the functionalization of bio-nanoconjugates [15]; and for the induction and inhibition of fibril formation [16]. Such a range of possible applications of albumin is due to both

the availability and low cost of SA and the relative completeness of knowledge [17,18] of their conformational state, intermolecular interaction, and phase behavior in dispersions with different microenvironments. This allows it to be an ideal object for studying the effect of proteins on the colloidal stability of nanoparticles in dispersion [19]. In turn, the aggregation and phase states of NPs can significantly affect their toxicity and possible mechanisms of drug delivery properties. Many solvent parameters affect colloidal stability, the state of the water hydrogen bond network being one of the most important, but this is not entirely clear.

Stable aqueous dispersions of shungite carbon nanoparticles (ShC NPs) and quartz nanoparticles (Qz NPs) are the objects in the study of the interaction mediated by hydrogen bonds with biological molecules. The natural origin of shungite carbon, its structural properties, and its physicochemical features of the main basic elements of ShC NPs with the properties of reduced graphene oxide were described earlier [20–25]. The study of structural–dynamic, hydrodynamic, thermodynamic, and redox properties of ShC NPs (and, to a lesser extent, Qz NPs) bio-nanoconjugates with albumin and its associates was carried out earlier by the methods of gel filtration chromatography, differential scanning calorimetry (DSC), electron paramagnetic resonance (EPR) of spin labels and spin probes, dynamic light scattering (DLS), and Raman scattering (RS) [26,27]. The role of ShC NPs in the redistribution of fatty acids (FA) between protein fractions has been established. The formation of a bio-nano-boundary between bovine SA and ShC NPs was suggested to contribute a greater homogeneity of the FA-binding boundary, a decrease in the protein fractions and active sites on the protein surface that are responsible for the supramolecular heterogeneity of the protein in the solution. In the case of ShC NPs, this is explained by the transition of ligands (FA) from SA molecules to graphene-like carbons with a corresponding change in the ratio of SA fractions with different ligand contents.

Despite the fact that the main mechanisms of interaction and colloidal stability in nanoparticle–protein systems are implemented through water, its role has not yet been disclosed. This is not surprising, since the cluster structure of ordinary water is one of the most difficult problems of modern science [28]. In this case, the system of hydrogen bonds can determine and regulate the balance of forces, promoting either the disaggregation or complex formation of components, depending on the presence and state of defects in the water structure [29]. Dissolved components can affect the network of hydrogen bonds in water, being located in its defects. This can contribute both to its loosening and hardening [30], depending on the hydrophobic–hydrophilic balance. As a result, all sorts of non-linear effects can manifest themselves in the physicochemical properties of dispersions [19].

When studying the state of water hydrogen bonds in SA dispersions by Raman spectroscopy in the range of 3200–3600 cm^{-1}, we obtained data [29] where self-association of protein molecules and formation of their clusters were accompanied by a change in the ordering of hydrogen bonds. An earlier [31] structuring of interfacial water on silica surface studied by the sum frequency generation (SFG) vibrational spectroscopy was observed. However, after phase separation in the water–cyclohexane–silica system, induced by the addition of water above the critical concentration, the water-adsorption layer turned out to be less ordered and practically the same as that of bulk water. In [32], the attenuated SFG intensity at 3200 cm^{-1} after SA adsorption on silica was explained by the fact that interfacial water molecules became less ordered due to a decrease in the surface ζ-potential.

The association of protein molecules themselves, as well as nano-bio-conjugates, can be considered within the framework of the concepts of the cluster structure of protein dispersion and associated liquid–liquid phase transitions. The system of hydrogen bonds contributes to the formation of protein clusters if the size of the defects is suitable to accommodate them. Water in dispersions tends to arrange the elements of the system in the defects of its structure of various dimensions. As the main defects are filled, the network of hydrogen bonds of water stabilizes to such an extent that excess stresses are created in it and entropy decreases [28]. If the electronic structure of the particles dissolved in the dispersion contributes to the creation of new, larger defects, then the system of the hydrogen bonds

in water loosens again. In this case, defects can be filled with larger associates. However, abiogenic NPs in this case can serve as protein condensation centers with the formation of a protein corona, which probably promotes the loosening of hydrogen bonds to the optimal degree and maintains the colloidal stability of the NP–protein system.

In this regard, the main aim of this work was to investigate in more detail the possible effects of the joint impact of SA and NP ShC, as well as SA and Qz NPs obtained from shungite rocks, on the colloidal stability of mixed dispersions. In this case, the ligand state of the protein was taken into account when interacting with FA, which affects SA conformation and fractional composition. The method of Raman scattering was used to record the spectra of mixed dispersions of NPs and proteins in the range of wave numbers 3200–3600 cm^{-1} due to OH stretching vibrations in the network of water hydrogen bonds. Changes in the sizes of associates arising as a result of the interaction were controlled by dynamic light scattering. Changes in the morphology of associates were recorded by examining condensate films of mixed dispersions using a 3D laser microscopy.

2. Materials and Methods

2.1. Materials

2.1.1. Aqueous Dispersions of Shungite Carbon Nanoparticles

In the experiments, we used stable aqueous dispersions of ShC NPs prepared using the original procedure on the basis of the carbon-rich shungite rock (Shungite type I, 96 wt.% carbon). Samples were ground to powder with an average particle size of less than 40 μm. Shungite powder was subjected to treatment several times by water with stirring and followed by filtration. Ultrasonic treatment (frequency 22 kHz, power 300 W) was followed by filtration and ultracentrifugation. While using this original method [33], prepared dispersions were characterized by a nanoparticle concentration of 0.1 mg/mL, pH 6.5. According to atomic absorption spectrometry and mass spectrometry with inductively coupled plasma, the primary shungite powder contained non-carbon elements in an amount of no more than 0.3 μg/mL, with the exception of Na, the level of which was below 2 μg/mL. No traces of these chemical elements were found in the aqueous dispersion of ShC NPs. Transmission electron microscopy did not allow us to detect other carbon particles or agglomerations, except for ShC NPs. Judging by the maxima of the size distribution of dynamic light scattering intensity using the Malvern Zetasizer analyzer, NPs had a radius of 51 ± 7 nm with a distribution peak 20 nm wide and a polydispersity index of 0.201 ± 0.070. In this case, the measured value of the ζ-potential was −30 mV, which indicates a satisfactory stability of the dispersion. As follows from the data of scanning electron microscopy, the above procedure for processing ShC allows one to obtain dispersions of carbon NPs with the original structure of preserved shungite carbon. It should be noted that the results presented here will not necessarily apply to ShC NPs dispersions that are produced using other technologies.

The initial dispersions thus obtained were characterized by ultraviolet-visible (UV-Vis) (SP-56, OKB Spectr LOMO, Saint-Petersburg, Russia), Raman (Nicolet Almega XR spectrometer, Thermo Scientific, Madison, WI, USA), and DLS (Zetasizer Nano ZS, Malvern Instruments Ltd., Malvern, UK) spectrometry. The whole Raman spectra of the dispersions are given in Figure 1. The UV absorption spectrum of such a dispersion with a characteristic peak at 256 nm, when compared with the spectra of graphene oxide and reduced graphene oxide [34,35], allows us to assume that ShC in the dispersion has a degree of oxidation close to reduced graphene oxide [36].
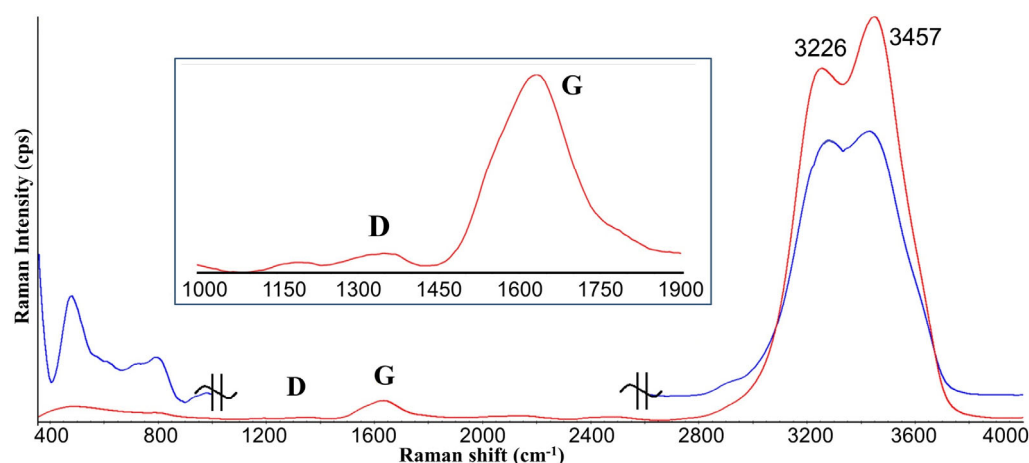
Figure 1. Raman spectra of shungite carbon (ShC) nanoparticles in aqueous dispersion (red) and quartz (Qz) nanoparticles in aqueous dispersion (blue). Nanoparticles content 0.12 mg/mL. Insertion: the first order region of Raman spectrum with the typical D and G bands of carbon materials. ID/IG— 0.04. (The signal intensities of the Raman spectra of Qz NPs dispersion in the region 400–1000 cm^{-1} was increased ten-fold to guide the eyes).

2.1.2. Aqueous Dispersions of Quartz Nanoparticles

To obtain stable aqueous dispersions of quartz NPs, samples of vein crystalline quartz of shungite rocks (Qz, 98 wt.%) from the Zazhogino deposit (Karelia) and the developed technique [37] were used. Samples were ground in a ball mill to a powder with a particle size of less than 50 μm, held in water at a ratio of 1:10 for 24 h, filtered, and then treated with 300 W ultrasound at a frequency of 22 kHz in water. The resulting dispersion was filtered, diluted with distilled water to a concentration of 0.1 mg/mL, and centrifuged at 3000 rpm. The supernatant dispersion was dried. The phase of α-quartz was determined for nanoparticles using X-ray study. Stable aqueous dispersions of quartz NPs (ζ-potential, 25 mV) were obtained at minimum powder concentrations of 0.1 mg/mL with an average size of quartz particles in the dispersion of 120 nm (nanosized α-quartz).

The Raman spectra of all studied samples of Qz NPs in aqueous dispersion showed that the main component of the samples is crystalline α-quartz; however, the spectra also contain peaks that are characteristic of graphene-like carbon (Figure 1). A weak signal or the absence of a D peak in the spectrum of quartz NPs indicates that quartz NPs are covered with carbon film. In the film deposited from the dispersion after centrifugation, the particles have a globular shape and form spatial aggregates. Stable aqueous dispersions of Qz NPs have a pH close to neutral. The colloidal stability and average size of NPs in dispersions can be controlled by changing the powder/water ratio at the stage of obtaining a dispersion. Centrifugation makes it possible to obtain a narrower particle size distribution and structure NPs in spatial aggregates during dispersion condensation. The initial stable aqueous dispersions of Qz NPs had a concentration of 0.32 mg/mL. The size of NPs was determined from the maxima of the size distribution curve of the DLS intensity. Aqueous dispersion of commercial nanodispersed amorphous silicon dioxide ("white carbon" BS-50) was used as a reference sample.

We used commercial albumin preparations from Sigma: both fatty-free (BSA_{faf}) and native, containing physiological amount of FAs (fraction V). This fraction (BSA_{5fr}) contains about 1.5 mol of FAs per mol of protein [38]. Cluster effects of quartz NPs and ShC were studied in relation to bovine serum albumin, both BSA_{5fr} and BSA_{faf}, in aqueous dispersions at different concentrations of protein and nanoparticles.

A solution of BSA in distilled water with a concentration of 0.02 to 20 mg/mLwas added to a dispersion of ShC or Qz nanoparticles in the same water (the initial concentration of ShC nanoparticles was 0.05; 0.1 mg/mL) in a ratio of 1:1, thoroughly mixed, and kept for

at least 3 h before experiments. The resulting mixtures were uniform in color and remained stable over time.

Dispersion condensates were obtained from a stable aqueous dispersion of ShC NPs and a mixture of ShC NPs with protein by depositing them on a glass substrate in the form of films and completely evaporating water on a fan (temperature ~40 °C).

2.2. Methods

The solvent-mediated interaction of nanoparticles with protein molecules was studied using a Nicolet Almega XR Raman spectrometer equipped with a 532 nm laser with a spectral resolution above 1 cm^{-1}. The power of the exciting laser at this wavelength was 15 mW. The spectra were recorded with a 30 min accumulation. The dispersions were placed in a quartz cuvette, which was installed in the compartment for macro samples perpendicular to the laser beam axis. The temperature of the sample was 22 °C and it did not change over the laser. The Raman spectrum was obtained by excitation of the sample (dispersion of nanoparticles) at 532 nm, followed by measurements of the frequency and intensity of the scattered light. Changes in the position, intensity, and width of the Raman peaks in the spectral region 3000–3600 cm^{-1}, which characterize the state of the water hydrogen bond system, were evaluated [39–41]. Raman spectral data such as maximum peak position and peak band width were determined using OMNIC software (8.2). The bands in the spectra are approximated by Gaussian functions. The line asymmetry was taken into account as a result of the approximation of the spectra by three Gaussian functions. The products of the amplitude I of the Gaussian maxima and the band width S were calculated and their ratio d = IS(3450 cm^{-1})/IS(3250 cm^{-1}) was used. Accounting for the bandwidth S does not change the general trends in the behavior of the I(3450 cm^{-1})/I(3250 cm^{-1}) parameter, but allows for minimizing the measurement error.

The effect of NPs on the formation of aggregates and associates in a BSA solution was evaluated by dynamic light scattering (DLS) using a Zetasizer Nano ZS particle size and zeta potential analyzer equipped with a helium–neon laser with a wavelength of 633 nm and a scattering angle 173°. The DLS data were processed using the standard "Protein analysis" procedure of the Malvern Zetasizer software 6.01.

The surface and thickness of the resulting films were examined on a Keyence scanning laser 3D-microscope VK-9700K (Keyence Corp., Osaka, Japan), which operates on a semiconductor violet laser with a wavelength of 408 nm and a power of 0.9 mW.

3. Results

Despite the large factual material on the Raman spectroscopy of water in the range of 3000–3600 cm^{-1}, there is still no consensus on the identity of the number of sub-ranges of the stretching vibrations of OH bonds in water. Deconvolution of the water spectrum in this region makes it possible to distinguish five characteristic frequencies, the most intense of which are two frequencies, 3230 and 3440 cm^{-1}. They correspond to 90% of the state of water [42,43]. The former is believed to characterize the symmetric mode of OH stretching vibrations in the network of bonds of water molecules in the state of two donors–two acceptors (DDAA–OH), and the latter characterizes the asymmetric mode of water in the donor–acceptor state (DA–OH). This division is somewhat arbitrary, since the bulk of water molecules still form three bonds. Nevertheless, the intensity ratio (I) of the I(3440 cm^{-1})/I(3230 cm^{-1}) peaks in terms of (DA–OH)/(DDAA–OH) makes it possible to evaluate the change in the orientational ordering of water molecules involved in less and more strongly bound fragments of a network of hydrogen bonds. A decrease in this ratio correlates with the strengthening of hydrogen bonds, while an increase correlates with the loosening of hydrogen bonds.

At the same time, dissolved substances or temperature variations can change the frequency values [44]. Thus, in the presence of hydrated tissues of biological origin or bio-macromolecules, the positions of the peaks shift to the region of 3450 and 3250 cm^{-1} [41,43].

Figure 2 shows the state of the network of hydrogen bonds in water under the changes in the concentration of nanoparticles of shungite carbon, quartz, and serum albumin in various ligand states, i.e., in the absence and in the presence of fatty acids.
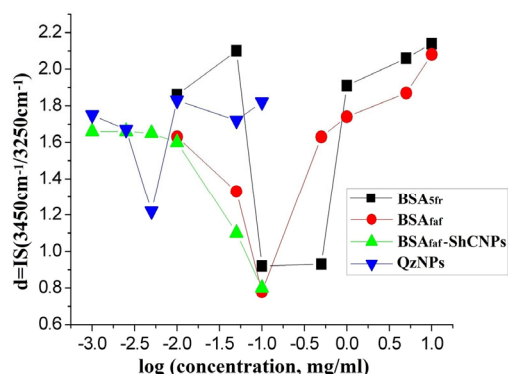

Figure 2. Changes in the ratio of the parameter d= IS(3450 cm^{-1})/IS(3250 cm^{-1}) of the Raman spectra in the range of 3000–3650 cm^{-1} on the concentration of dispersion components (as a logarithm of the concentration, in mg/mL). Bovine serum albumin (BSA) protein in various ligand states, top to bottom: BSA$_{5fr}$; BSA$_{faf}$; ShC NPs; and Qz NPs. The relative error in determining the ratio did not exceed 10%.

In stable dispersions (at large values of the zeta potential $\zeta < -30$ and at low concentrations of components), the state of the hydrogen bond network does not fundamentally differ for all the systems studied and is characterized by the relative value d = IS(3450 cm^{-1})/IS(3250 cm^{-1}) $\approx 1.9 \pm 0.2$. However, an increase in the ShC NPs concentration leads to the fact that the network of water bonds is first strengthened (the parameter d = IS(3450 cm^{-1})/IS(3250 cm^{-1}) decreases to 0.9), apparently due to the contribution of the increasing hydrophobic surface of nanoparticles and possible semi-clathrate hydration. It is likely that ShC NPs at this concentration filled the existing defects in the hydrogen bond network, and so, new defects of a larger size could not be created due to the features of the electronic structure of ShC. As a result, at a concentration of ShC NPs > 0.1 mg/mL, the limit of colloidal solubility of carbon nanoparticles sets in, the stability of the system is violated, and a cloudy black precipitate appears. Thus, excessive strengthening of the hydrogen bond network, which is usually observed in the presence of nonpolar molecules that form clathrates [40], leads to a violation of the colloidal stability of the dispersion.

Similarly, the initial strengthening of the hydrogen bond network (parameter d = IS(3450)/IS(3250)~ 0.9) with an increase in the protein concentration to 0.1 mg/mL in Figure 2 can also be associated with the onset of thermodynamic destabilization of the molecular solution due to the filling of primary defects of the hydrogen bond network with protein molecules. In this case, the destabilization does not end with a macroscopic phase transition. Perhaps this is due to the fact that protein molecules that are more polar than ShC NPs have the ability both to stabilize the system of water bonds and to destroy it, creating structural defects of a large size. These defects can be filled with associates of metastable protein clusters.

The data on particle sizes in SA solutions at different protein concentrations have been obtained from the curves of the light scattering intensity distribution by particle size using the DLS method. They contain, as a rule, three peaks (Figure 3, red). The first can obviously be attributed to protein molecules and their minor associates (dimers and trimers), ranging in size from 2 to 10 nm. The second and third correspond to the protein associates ranging in size from 20 to 80 nm and from 200 to 800 nm. The theory of DLS is that the intensity of light scattered by particles whose size is comparable to the light wavelength depends very strongly on the particle diameter; it is the sixth power of the diameter of the spherical particles. Thus, the scattering of larger particles masks the scattering of smaller ones, even when the number of the former is less than the number of the latter. Accordingly, the data imply that the number of single-protein molecules exceeds the number of associates of

both types by several orders of magnitude, and the number of smaller associates is many times greater than the number of large ones at all protein concentrations. It means that for each NP in the dispersion, there is a number of protein molecules many times greater than that which forms the protein corona of NPs in association with NPs and BSA. It should be noted that the maximum of the intensity distribution is determined by the particles, the combination of size and number of which gives the highest total scattering intensity.
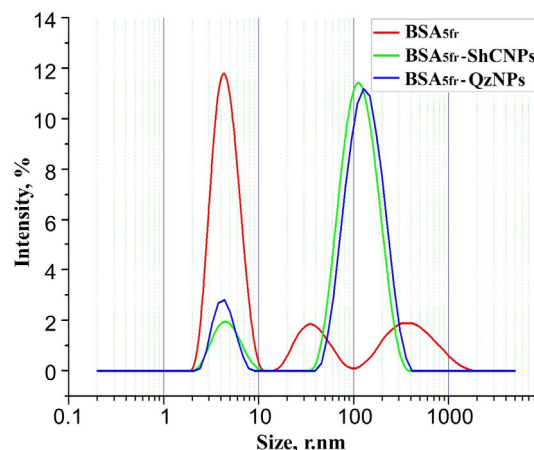

Figure 3. Examples of the dynamic light scattering (DLS) data on the distribution of the relative intensity of scattered light by particle size (Stokes diameter) for native BSA_{5fr} (containing fatty acids, fraction V) at concentration 30 mg/mL in 0.2 M phosphate-buffer solution (pH 5.2) (red), in 0.035 mg/mL ShC dispersion (green), and in 0.67 mg/mL quartz dispersion (blue) at 25 °C.

The size of larger protein associates is presented in Figure 4 as a Stokes diameter determined by the maximum values of the corresponding peak in the distribution by the particle size of scattered light intensity. Figure 4 shows that the dependence of the size of protein nano- and submicron SA associates on the protein concentration is increasing for the larger protein associates and is absent for smaller protein associates. No changes were observed for the first peak related to single-protein molecules (not shown in Figure 4). This apparently means that colloidal stability of dispersions in both cases occurs due to an increase in the size of the largest particles. At the same time, the phenomenon of strengthening the hydrogen bond network due to the filling of primary defects is compensated by the formation of secondary defects. In this case, the system reaches the previous level of energy stability with a more loosened network of hydrogen bonds (parameter d = IS(3450 cm^{-1})/IS(3250 cm^{-1}) ~ 1.8 ± 0.2) by forming a supramolecular cluster organization. At the same time, in the dispersion of fatty acid-free proteins, the stabilization effect begins in the region of lower protein concentrations than in the SA_{5fr} protein dispersion (Figure 2). This can be explained by conformational (or electronic) differences between the ligand and non-ligand forms of the protein.

Thus, it can be assumed that, along with the filling of initial defects with small clusters, relatively polar molecules are able to induce the formation of larger defects in the hydrogen bond network, for which large associates of molecules are more suitable for filling.

Quartz NPs, which are stable at higher concentrations than ShC, affect the state of water hydrogen bonds in the same way as proteins (Figure 2). The effect of strengthening the network of hydrogen bonds in their dispersion begins to be observed at very low concentrations of Qz NPs. With an increase in the concentration of quartz NPs to more than 0.005 mg/mL, the established bond structure begins to loosen (the parameter d = IS(3450 cm^{-1})/IS(3250 cm^{-1}) increases) and again, reaches the initial level d ~1.8 ± 0.2. In this case, the colloidal stability of the quartz dispersion is not disturbed and is maintained at least up to concentrations of 0.3–0.6 mg/mL.
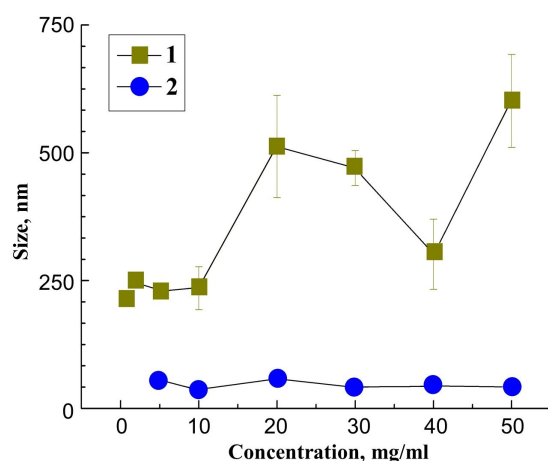
Figure 4. Hydrodynamic size of larger protein (squares) and smaller protein (circles) associates of BSA$_{5fr}$ molecules, containing physiological amount of fatty acids (native) in the dispersion based on 0.2 M phosphate-buffer solution (pH 5.2) at 25 °C depending on protein concentration.

Thus, in such a seemingly and completely different system to the dispersion of carbon nanoparticles, quartz, and protein macromolecules, a generally similar behavior of the hydrogen bond network is observed with a change in the concentration of components: initial strengthening and further loosening. In this regard, it is of interest to study the mutual influence of some elements of the dispersion that capable of cluster self-regulation, ShC NPs and Qz NPs, on the same properties of protein macromolecules.

Figure 5 shows changes in the network of hydrogen bonds of water in mixed dispersions of fatty acid-free and native BSA$_{5fr}$ in the presence of ShC NPs and Qz NPs with a change in protein concentration. Thus, for fatty acid-free proteins, under the effect of ShC NPs, the weak stabilization of bonds in the range of protein concentrations of 0.1–1 mg/mL have been observed. It is replaced by loosening, with a further increase in the protein concentration. At the same time, for the native protein, no changes in the system of hydrogen bonds are observed over the entire range of concentrations. This may be due to the fact that ShC changes the nature of the association of protein molecules.
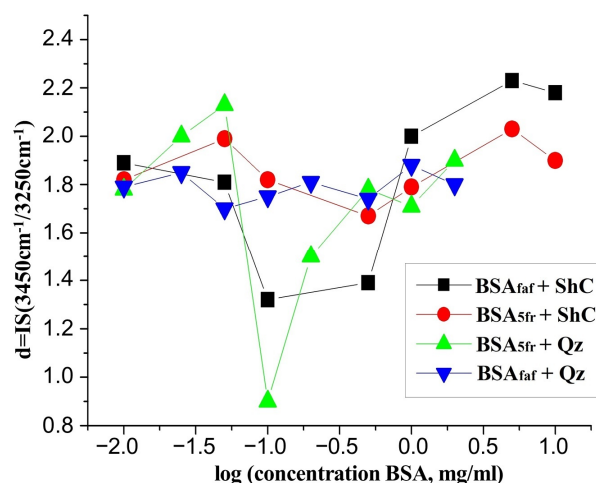

Figure 5. Change in the ratio of the parameter d = IS(3450 cm^{-1})/IS(3250 cm^{-1}) of the Raman spectra of albumin protein (BSA) dispersions depending on the concentration in the presence of nanoparticles of ShC and Qz, top to bottom:fatty acid-free BSA$_{faf}$ + ShC;native BSA$_{5fr}$ + ShC;native BSA$_{5fr}$ + Qz; and fatty acid-free BSA$_{faf}$ + Qz. The relative error in determining the ratio did not exceed 10%.

Figure 6 shows data on the hydrodynamic size of associates of ShC NPs and native BSA$_{5fr}$ depending on the protein concentration. They were obtained from the light scat-

tering intensity distribution curves by the DLS method. According to the primary data, NP–protein associates give nonzero scattering intensity in the region of 40–300 nm (the whole width of the peak) at the studied protein concentrations with a distribution maximum at the values presented in Figure 6. There is also a peak in the scattering intensity distribution in the range of 2–7 nm, which clearly belongs to single-protein molecules. The position of its maximum does not differ for various protein concentrations.Their size may differ from the size of those particles, the number of which is the maximum. The size of the associates increases with the rising protein concentration by approximately 20–25 nm, which is obviously the thickness of the protein corona layer of the ShC NP at the maximum concentration. The formation of a protein corona in the presence of nanoparticles is a well-known and studied phenomenon [7,8]. In this case, protein molecules can pass into the corona both individually and as part of oligomers, the latter phenomenon being more preferable [13,45].
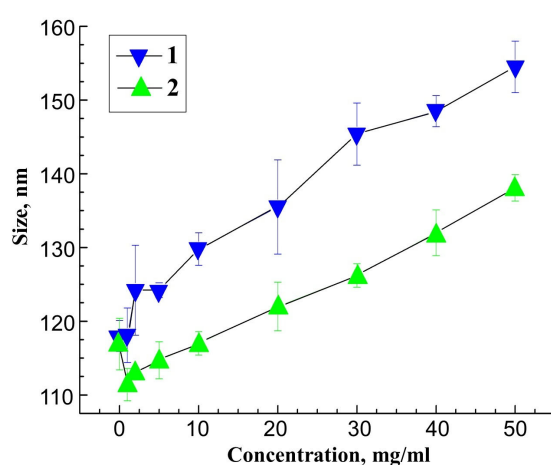

Figure 6. Hydrodynamic size of associates of quartz NPs + native BSA_{5fr} (1) and of NPs ShC + native BSA_{5fr} (2) in a dispersion based on 0.2 M phosphate-buffer solution (pH 5.2) at 25 °C plotted against protein concentration. ShC concentration 0.025 mg/mL and Qz NP concentration 0.67 mg/mL.

Native BSA is well-known to be more structurally stable and compact than fatty acid-free BSA. This clearly can affect their adsorption pattern on ShC and Qz. However, based on the size of NPs, HSA molecules, and the assumption of few layer adsorptions, it turns out that the nanoparticle surface is accessible only to a negligible fraction of the total protein in the dispersion. All this does not allow us to expect that even large changes in the structure of such a small fraction of the protein upon such contact will lead to the observed significant changes in the effect.

Using differential scanning microcalorimetry, we found [27] that the affinity of fatty acid-free BSA_{faf} for ShC is higher than for each other, i.e., the BSA_{faf} state is shifted towards a less-associated state in the presence of ShC. Due to the presence of protein monomers, a partial stabilization of the network of hydrogen bonds of water occurs, which is noticeable in Figure 5 by a decrease in the parameter d to 1.3 ± 0.1 in the protein concentration range of 0.1–0.5 mg/mL. The fatty acid-free BSA_{faf} molecules begin to associate again only after the formation of the protein corona. Therefore, only with a further increase in the protein concentration, self-association begins, which is accompanied by a loosening of the OH bonds of water.

In the dispersions of native BSA_{5fr} in the presence of ShC, no destruction of protein clusters occurs, since the affinity of protein molecules to ShC does not differ from each other. In this case, the protein corona is formed mainly from a dispersion of monomers, which slightly affects the protein associates. Because of this, the stabilization of the hydrogen bond network is not observed in the entire range of the studied concentrations of the BSA_{5fr} (Figure 5).

Judging by Figure 5, in the presence of Qz NPs, no changes in the state of the hydrogen bonds are observed over the entire range of the fatty acid-free BSA_{faf} concentrations that are studied, just as it occurs in the presence of ShC NPs + native BSA_{5fr}. This may be due to the fact that the corona created by protein molecules around Qz NPs is much larger than in the case of ShC, while significantly more protein molecules are involved in the creation of the corona. Moreover, the oligomeric form of the protein state is more adhesive with respect to Qz NPs than the monomeric one [13]. In turn, oligomerization occurs more intensively for fatty acid-free BSA_{faf} molecules, and its rate increases with increasing temperature [45]. It is possible that after the formation of the corona, the predominantly oligomeric protein remains in the dispersion, but in its presence, the strengthening of the hydrogen bond system does not occur.

At the same time, for the BSA_{5fr}+ Qz NPs, a significant strengthening of OH bonds has been observed at a protein concentration of 0.1 mg/mL, followed by a return to the initial loosening state at high protein concentrations. This may be due to the fact that the BSA_{5fr} consists of two subfractions, the molecules of which are more and less loaded with FAs [46]. In this case, one of the albumin subfractions, which is more loaded with FA, is included in the protein corona, while the less loaded subfraction remains in the dispersion and stabilizes the hydrogen bond system. With an increase in the total concentration of the BSA_{5fr}, aggregation of the protein of this subfraction may occur, which is accompanied by further loosening of the hydrogen bond network.

Figure 6 shows data on the hydrodynamic size of Qz NP + native BSA_{5fr} associates, depending on the protein concentration. The corresponding primary intensity distributions of light scattering by the DLS method contain, as in the case of ShC NP, two peaks: the first one peak contains single-protein molecules the size of 2–7 nm, and the second one contains associates of NPs with protein molecules the size of 50–300 nm. The general nature of the dependences is similar to that observed for ShC NP. The size of associates increases by approximately 28–33 nm, which reflects the thickness of the layer of the protein corona of Qz NPs at the maximum protein concentration.

Thus, the results obtained allow us to conclude that the emerging instability in protein dispersions due to the initial excessive strengthening of hydrogen bonds is compensated by the formation of protein aggregates of various types and sizes with increasing protein concentrations. This phenomenon can be considered analogous to a phase transition of the L–L type, while clusters of a new, "hidden" phase can be in metastable equilibrium with a dispersion of monomers, since they are stabilized by the difference in capillary pressures on the cluster and monomer [47]. In turn, the existence of different protein fractions promotes phase formation [48].

In the presence of nanoparticles in a dispersion with a protein, the initial stabilization of hydrogen bonds is compensated mainly due to the association of protein molecules with NPs, which becomes the regulating factor of the cluster state of mixed dispersions. At the same time, aggregation structures arising in mixed-protein dispersions with NPs should differ for proteins in different ligand states, due to differences in the strength of interaction between NPs and the protein surface in the region of ligand-binding centers. To confirm this, images of films of condensates of protein dispersions with ShC NPs were studied.

Figure 7 shows 2D and 3D images of the surface of the condensate film of native BSA_{5fr} and fatty acid-free BSA_{faf} with ShC, precipitated at different concentrations of protein and ShC, and taken with a confocal 3D microscope (Figure 7a,b). It can be seen that the aggregates of hybrid nanoparticles with protein in the films of condensates differ significantly in shape and size. Native proteins form spatial structures that transform into 3D networks with an increase in the thickness of the condensate film (Figure 7a). More dense and disparate aggregates form hybrids based on fatty acid-free proteins (Figure 7b). With a decrease in the concentration of fatty acid-free BSA_{faf} and ShC NPs in the dispersion, the density and shape of the aggregates of the hybrid nanoparticles change (Figure 7c).
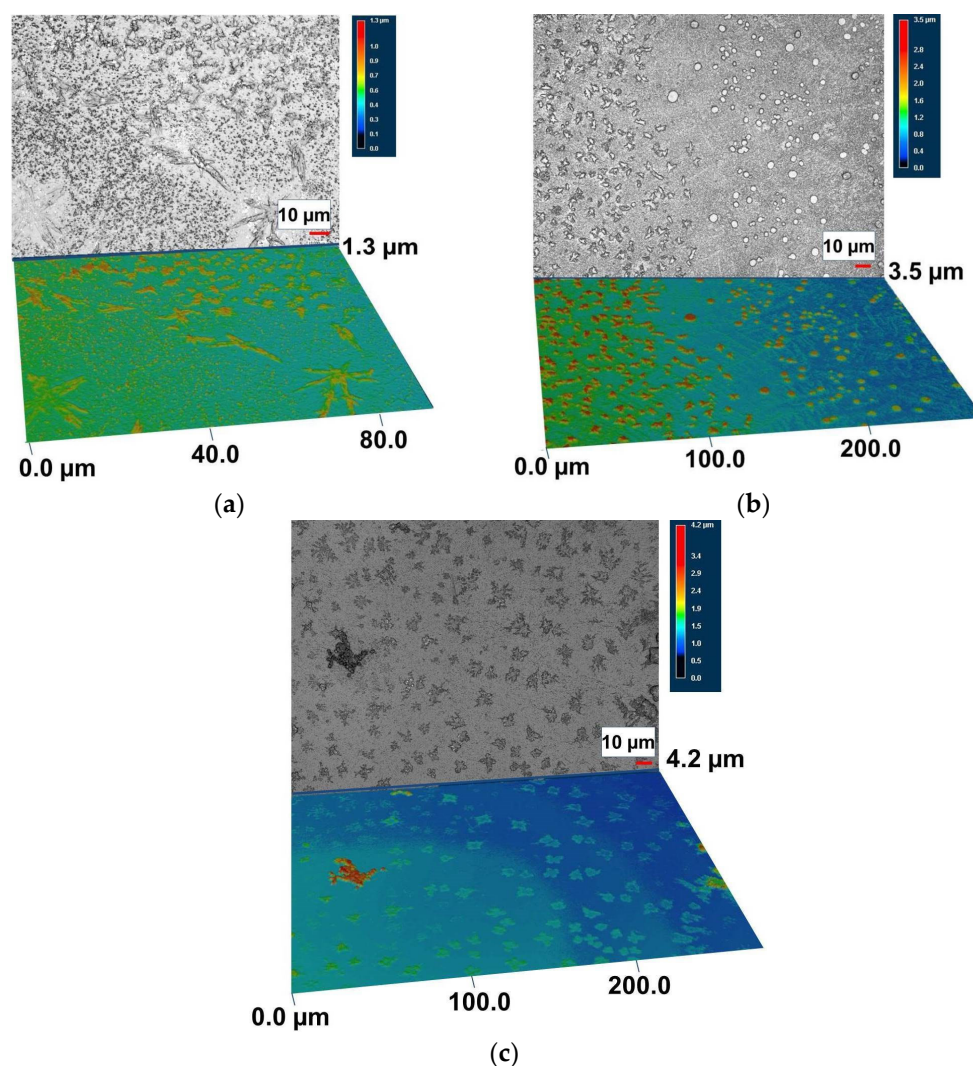
Figure 7. 2D and 3D (**a**,**b**) images of the surface of condensate films of a hybrid of native BSA$_{5fr}$ (0.05 mg/mL) + ShC(0.05 mg/mL) (**a**) and fatty acid-free BSA$_{faf}$ (0.05 mg/mL) + ShC(0.05 mg/mL) (**b**). The films consist of particles of various shapes, assembled in short chains (**a**) and separate standing (**b**). Fatty acid-free BSA$_{faf}$ (0.025 mg/mL) + ShC (0.025 mg/mL) (**c**).

It follows from the above data on condensation structures that, depending on the presence of fatty acids, the morphology of condensation structures and the spatial aggregation of dispersion components change. The native protein with ShC NPs forms less associated aggregates with the signs of anisotropy of interaction between them, which are capable of further forming networks. The fatty acid-free proteins with ShC form larger and denser weakly interacting aggregates. In this case, the aggregates of fatty acid-free proteins with ShC decompose into individual hybrid nanoparticles when water is added.

4. Conclusions

The effects of water hydrogen bonds have been revealed in the formation of associates and condensates in dispersions of serum albumin with shungite carbon and quartz nanoparticles. In such seemingly and completely different systems for the dispersions of ShC NPs, quartz NPs, and SA, the Raman spectroscopy method observes a generally uniform behavior of the hydrogen bond network with a change in the concentration of components: its initial strengthening and subsequent loosening. As revealed by the DLS method, the primary associates that arise in this case have, on average, a close size and do not change with an increase in the concentration of the components. This may indicate

that the primary defects in the hydrogen bond network are filled with protein molecules or the basic elements of ShC, but then larger defects are formed and they can accept larger associates. In this case, the system of hydrogen bonds is loosened. In protein dispersion, colloidal stability and phase separation are maintained by the formation of protein associates (clusters) of two main types and sizes as latent phase clusters. In the presence of ShC and quartz NPs, the colloidal stability of the dispersion is provided almost exclusively by the association of the protein with the NPs and the formation of a protein corona. This approach can be used to describe the colloidal properties and stable behavior of nanoparticle–protein complexes and associates as pre-nuclear amorphous clusters [49] of an intermediate (hidden) phase. Such formations are typical not only for the world of bio-polymers and nanoparticles [50,51], but also for water-containing minerals [52].

Author Contributions: Conceptualization, and writing—original draft preparation, N.R.; special nanoparticle tests, design of the figures, L.P.; Raman study assistance, confocal laser 3D-microscope study: V.K.; dynamic light scattering measurements, analysis, writing, A.G.; conceptualization, methodology, and writing—original draft preparation, S.R. All authors have read and agreed to the published version of the manuscript.

Institutional Review Board Statement: Not applicable.

Informed Consent Statement: Not applicable.

Data Availability Statement: Not applicable.

Conflicts of Interest: The authors declare no conflict of interest.

References

1. Wang, Y.; Cai, R.; Chen, C. The Nano-Bio Interactions of Nanomedicines: Understanding the Biochemical Driving Forces and Redox Reactions. *Acc. Chem. Res.* **2019**, *52*, 1507–1518. [CrossRef]
2. Kopac, T. Protein corona, understanding the nanoparticle-protein interactions and future perspectives: A critical review. *Int. J. Biol. Macromol.* **2021**, *169*, 290–301. [CrossRef] [PubMed]
3. Marichal, L.; Giraudon-Colas, G.; Cousin, F.; Thill, A.; Labarre, J.; Boulard, Y.; Aude, J.C.; Pin, S.; Renault, J.P. Protein-Nanoparticle Interactions: What Are the Protein-Corona Thickness and Organization? *Langmuir* **2019**, *35*, 10831–10837. [CrossRef] [PubMed]
4. Mahmoudi, M.; Lynch, I.; Ejtehadi, M.R.; Monopoli, M.P.; Baldelli Bombelli, F.; Laurent, S. Protein-Nanoparticle Interactions: Opportunities and Challenges. *Chem. Rev.* **2011**, *111*, 5610–5637. [CrossRef] [PubMed]
5. Nasser, F.; Constantinou, J.; Lynch, I. Nanomaterials in the Environment Acquire an "Eco-Corona" Impacting their Toxicity to *Daphnia Magna*—A Call for Updating Toxicity Testing Policies. *Proteomics* **2020**, *20*, 1800412. [CrossRef] [PubMed]
6. Vitale, S.; Rampazzo, E.; Hiebner, D.; Devlin, H.; Quinn, L.; Prodi, L.; Casey, E. Interaction between Engineered Pluronic Silica Nanoparticles and Bacterial Biofilms: Elucidating the Role of Nanoparticle Surface Chemistry and EPS Matrix. *ACS Appl. Mater. Interfaces* **2022**, *14*, 34502–34512. [CrossRef]
7. Lundqvist, M.; Stigler, J.; Elia, G.; Lynch, I.; Cedervall, T.; Dawson, K.A. Nanoparticle size and surface properties determine the protein corona with possible implications for biological impacts. *Proc. Natl. Acad. Sci. USA* **2008**, *105*, 14265–14270.
8. Monopoli, M.P.; Walczyk, D.; Campbell, A.; Elia, G.; Lynch, I.; Baldelli Bombelli, F.; Dawson, K.A. Physical-Chemical Aspects of Protein Corona: Relevance to in Vitro and in Vivo Biological Impacts of Nanoparticles. *J. Am. Chem. Soc.* **2011**, *133*, 2525–2534. [CrossRef]
9. Philippe, A.; Schaumann, G.E. Interactions of Dissolved Organic Matter with Natural and Engineered Inorganic Colloids: A Review. *Environ. Sci. Technol.* **2014**, *48*, 8946–8962. [CrossRef]
10. He, J.Z.; Li, C.C.; Wang, D.J.; Zhou, D.M. Biofilms and extracellular polymeric substances mediate the transport of graphene oxide nanoparticles in saturated porous media. *J. Hazard. Mater.* **2015**, *300*, 467–474.
11. Treuel, L.; Brandholt, S.; Maffre, P. Impact of Protein Modification on the Protein Corona on Nanoparticles and Nanoparticle-Cell Interactions. *ACS Nano* **2014**, *8*, 503–513. [CrossRef]
12. Schuberta, J.; Chanana, M. Coating Matters: Review on Colloidal Stability of Nanoparticles with Biocompatible Coatings in Biological Media, Living Cells and Organisms. *Curr. Med. Chem.* **2018**, *25*, 4553–4586. [CrossRef] [PubMed]
13. Park, J.H.; Jackman, J.A.; Ferhan, A.R.; Ma, G.J.; Yoon, B.K.; Cho, N.J. Temperature-Induced Denaturation of BSA Protein Molecules for Improved Surface Passivation Coatings. *ACS Appl. Mater. Interfaces* **2018**, *10*, 32047–32057. [CrossRef] [PubMed]

14. Otzen, D.E. Proteins in a brave new surfactant world. *Curr. Opin. Colloid Interface Sci.* **2015**, *20*, 161–169. [CrossRef]

15. Li, D.; Zhang, W.; Yu, X.; Wang, Z.; Su, Z.; Wei, G. When biomolecules meet graphene: From molecule-level interactions to material design and applications. *Nanoscale* **2016**, *8*, 19491–19509. [CrossRef] [PubMed]

16. Zaman, M.; Ahmad, E.; Qadeer, A. Nanoparticles in relation to peptide and protein aggregation. *Int. J. Nanomed.* **2014**, *9*, 899–912.

17. Rosenoer, V.M.; Oratz, M.; Rothschild, M.A. (Eds.) *Albumin: Structure, Function and Uses*; Elsevier: Amsterdam, The Netherlands, 2014; 412p.

18. Peters, T., Jr. *All about Albumin: Biochemistry, Genetics and Medical Applications*; Academic Press, Inc.: San Diego, CA, USA, 1996; 432p.

19. Sun, B.; Zhang, Y.; Chen, W.; Wang, K.; Zhu, L. Concentration Dependent Effects of Bovine Serum Albumin on Graphene Oxide Colloidal Stability in Aquatic Environment. *Environ. Sci. Technol.* **2018**, *52*, 7212–7219. [CrossRef] [PubMed]

20. Rozhkova, N.N.; Rozhkov, S.P.; Goryunov, A.S. Natural Grapheme-Based Shungite Nanocarbon. In *Carbon Nanomaterials Sourcebook: Graphene, Fullerenes, Nanotubes, and Nanodiamonds*; Aliofkhazraei, M., Ali, N., Milne, W.I., Eds.; CRC Press Inc. (Taylor and Francis Group): Boka Raton, FL, USA; London, UK; New York, NY, USA, 2016; Volume 1, pp. 153–178.

21. Rozhkova, N.N. Aggregation and stabilization shungite carbon nanoparticles. *Russ. J. Gen. Chem.* **2013**, *4*, 240–251. [CrossRef]

22. Rozhkova, N.N.; Yemel'yanova, G.I.; Gorlenko, L.E.; Gribanov, A.V.; Lunin, V.V. From stable aqueous dispersion of carbon nanoparticles to the clusters of metastable shungite carbon. *Glass Phys. Chem.* **2011**, *37*, 613–618. [CrossRef]

23. Sheka, E.F.; Popova, N.A. Molecular theory of graphene oxide. *Phys. Chem. Chem. Phys.* **2013**, *15*, 13304–13322. [CrossRef]

24. Razbirin, B.S.; Rozhkova, N.N.; Sheka, E.F. Fractals of graphene quantum dots in photoluminescence of shungite. *JETP* **2014**, *118*, 735–746. [CrossRef]

25. Razbirin, B.S.; Rozhkova, N.N.; Sheka, E.F. Photonics of shungite quantum dots. In *Graphene Science Handbook: Electrical and Optical Properties*; Aliofkhazraei, M., Ali, N., Milne, W.I., Eds.; CRC Press Inc. (Taylor and Francis Group): Boka Raton, FL, USA; London, UK; New York, NY, USA, 2016; pp. 425–436.

26. Rozhkov, S.P.; Goryunov, A.S. Structural dynamic effects of protein and other biologically significant molecules interaction with shungite nanocarbon. *Trans. Karelian Res. Cent. Russ. Acd. Sci. Exp. Biol. Ser.* **2017**, *5*, 33–44. (In Russian)

27. Goryunov, A.; Rozhkov, S.; Rozhkova, N. Fatty acid transfer between serum albumins and shungite carbon nanoparticles and its effect on protein aggregation and association. *Eur. Biophys. J.* **2020**, *49*, 85–94. [CrossRef]

28. Gao, Y.; Fang, H.; Ni, K.; Feng, Y. Water clusters and density fluctuations in liquid water based on extended hierarchical clustering methods. *Sci.Rep.* **2022**, *12*, 8036. [CrossRef] [PubMed]

29. Rozhkov, S.P.; Goryunov, A.S.; Kolodey, V.A.; Pron'kina, L.A.; Rozhkova, N.N. Interaction between serum albumin molecules, fatty acids and graphenes of shungite carbon nanoparticles in aqueous dispersion based on raman spectroscopic analysis of water in the high wavenumber region. *Biophysics* **2022**, *67*, 884–890.

30. Chaban, I.A.; Rodnikova, M.N.; Zhakova, V.V. Concentration interval of destruction of the network of hydrogen bonds of water in aqueous solutions of non-electrolytes. *Biophysics* **1996**, *41*, 293–298. (In Russian)

31. Mizukami, M.; Kobayashi, A.; Kurihara, K. Structuring of interfacial water on silica surface in cyclohexane studied by surface forces measurement and sum frequency generation vibrational spectroscopy. *Langmuir* **2012**, *28*, 14284–14290. [CrossRef]

32. Kim, J.; Cremer, P.S. Elucidating changes in interfacial water structure upon protein adsorption. *Chem. Phys. Chem.* **2001**, *2*, 543–546. [CrossRef]

33. Institute of Geology of the Karelian Research Centre of the Russian Academy of Sciences. Method for Obtaining an Aqueous Dispersion of Carbon Nanoparticles from Shungite. Patent RF No. 2642632, 25 January 2018.

34. Gurunathan, S.; Han, J.W.; Dayem, A.A. Oxidative stress-mediated antibacterial activity of graphene oxide and reduced graphene oxide in Pseudomonas aeruginosa. *Int. J. Nanomed.* **2012**, *7*, 5901–5914. [CrossRef]

35. Choi, Y.-J.; Kim, E.; Han, J. A Novel Biomolecule-Mediated Reduction of Graphene Oxide: A Multifunctional Anti-Cancer Agent. *Molecules* **2016**, *21*, 375. [CrossRef]

36. Goryunov, A.S.; Borisova, A.G.; Rozhkov, S.S.; Rozhkova, N.N. Structural and Colloid Effects of Interaction between Shungite Carbon Nanoparticles and Linoleic Fatty Acid. *Curr. Nanosci.* **2023**, *19*, 68–75. [CrossRef]

37. Institute of Geology of the Karelian Research Centre of the Russian Academy of Sciences. Nanosized Quartz and Method of Its Production. Patent RF No. 2778691, 23 August 2022.

38. Michnik, A.; Michalik, K.; Drzazga, Z. Stability of bovine serum albumin at different pH. *J. Thermal Anal. Calorim.* **2005**, *80*, 399–406. [CrossRef]

39. Masson, L.E.; O'Brien, C.M.; Pence, I.J.; Herington, J.L.; Reese, J.; van Leeuwenf, T.G.; Mahadevan-Jansen, A. Dual excitation wavelength system for combined fingerprint and high wavenumber Raman spectroscopy. *Analyst* **2018**, *143*, 6049–6060. [CrossRef] [PubMed]

40. Baschenko, S.M.; Marchenko, L.S. On Raman spectra of water, its structure and dependence on temperature. *Semicond. Phys. QuantumElectron. Optoelectron.* **2011**, *14*, 77–79. [CrossRef]

41. Korepanov, V.I.; Hamaguchi, H. Ordered structures in liquid water as studied by Raman spectroscopy and the phonon confinement model. *Bull. Chem. Soc. Jpn.* **2019**, *92*, 1127–1130. [CrossRef]

42. Maeda, Y.; Kitano, H. The structure of water in polymer systems as revealed by Raman spectroscopy. *Spectrochim. Acta Part A* **1995**, *51*, 2433–2446. [CrossRef]

43. Burikov, S.; Dolenko, S.; Dolenko, T.; Patsaeva, S.; Yuzhakov, V. Decomposition of water Raman stretching band with a combination of optimization methods. *Mol. Phys.* **2010**, *108*, 739–747. [CrossRef]
44. Unal, M.; Akkus, O. Shortwave-infrared Raman spectroscopic classification of water fractions inarticular cartilage ex vivo. *J. Biomed. Opt.* **2018**, *23*, 1–11. [CrossRef]
45. Borzova, V.A.; Markossian, K.A.; Chebotareva, N.A.; Kleymenov, S.Y.; Poliansky, N.B.; Muranov, K.O.; Stein-Margolina, V.A.; Shubin, V.V.; Markov, D.I.; Kurganov, B.I. Kinetics of Thermal Denaturation and Aggregation of Bovine Serum Albumin. *PLoS ONE* **2016**, *11*, e0153495. [CrossRef]
46. Shrake, A.J.; Ross, P.D. Biphasic denaturation of human albumin due to ligand redistribution during unfolding. *J. Biol. Chem.* **1988**, *263*, 15392–15399. [CrossRef]
47. Rozhkov, S.P.; Goryunov, A.S. Possible phase effects in dispersion of a globular protein in the temperature range of the protein's native state. *Biophysics* **2022**, *67*, 876–883.
48. Bulone, D.; Martorana, V.; SanBiagio, P.L. Effects of intermediates on aggregation of native bovine serum albumin. *Biophys. Chem.* **2001**, *91*, 61–69. [CrossRef] [PubMed]
49. Gebauer, D.; Kellermeier, M.; Gale, J.D.; Bergstrom, L.; Cölfen, H. Pre-nucleation clusters as solute precursors in crystallization. *Chem. Soc. Rev.* **2014**, *43*, 2348–2371. [CrossRef] [PubMed]
50. Sauter, A.; Roosen-Runge, F.; Zhang, F.; Lotze, G.; Feoktystov, A.; Jacobs, R.; Schreiber, F. On the question of two-step nucleation in protein crystallization. *Faraday Discuss.* **2015**, *179*, 41–58. [CrossRef]
51. Nguyen, T.K.; Maclean, N.; Mahiddine, S. Mechanisms of Nucleation and Growth of Nanoparticles in Solution. *Chem. Rev.* **2014**, *114*, 7610–7630.
52. Askhabov, A.M. Pre-nucleation clusters and non-classical crystal formation. *Proc. Russ. Mineral. Soc.* **2019**, *148*, 1–13.